NASA Technical Memorandum 4693

Structural Optimization Methodology for Rotating Disks of Aircraft Engines

Sasan C. Armand

November 1995

National Aeronautics and
Space Administration

NASA Technical Memorandum 4693

Structural Optimization Methodology for Rotating Disks of Aircraft Engines

Sasan C. Armand
Lewis Research Center
Cleveland, Ohio

National Aeronautics and
Space Administration

Office of Management

Scientific and Technical
Information Program

1995

Summary

In support of the preliminary evaluation of various engine technologies, a methodology has been developed for structurally designing the rotating disks of an aircraft engine. The structural design methodology, along with a previously derived methodology for predicting low-cycle fatigue life, was implemented in a computer program. An interface computer program was also developed that gathers the required data from a flowpath analysis program (WATE) being used at NASA Lewis. The computer program developed for this study requires minimum interaction with the user, thus allowing engineers with varying backgrounds in aeropropulsion to successfully execute it. The stress analysis portion of the methodology and the computer program were verified by employing the finite element analysis method. The 10th-stage, high-pressure-compressor disk of the Energy Efficient Engine Program (E^3) engine was used to verify the stress analysis; the differences between the stresses and displacements obtained from the computer program developed for this study and from the finite element analysis were all below 3% for the problem solved. The computer program developed for this study was employed to structurally optimize the rotating disks of the E^3 high-pressure compressor. The rotating disks designed by the computer program in this study were approximately 26% lighter than calculated from the E^3 drawings. The methodology is presented herein.

Introduction

The first steps in evaluating a new propulsion concept are thermodynamics study and mission study. However, other areas, such as mechanical design, weight, and cost of the propulsion system, need to be examined before a final selection of the propulsion system is made. The methodology used in this study provides an easy-to-use, rapid, and accurate method of designing and calculating the weight of a homogeneous rotating disk. A typical rotating disk and blades are shown in figure 1.

A primary challenge in evaluating the necessary technology and thus identifying the designability of an aircraft gas turbine engine at the preliminary stages of an engine program is to determine the structural adequacy of the rotating disks because, generally, they experience the highest stress and temperature levels among engine components. Determining the adequacy of candidate engines in the areas of thermodynamics and mission is a relatively simple process. A similarly simple analysis tool to more completely evaluate the rotating disks and their structural adequacy would speed up the elimination process for engine candidates. The purpose of this study was to provide this analysis tool. With this tool the user can determine if the rotating disks can be designed within the limitations of current technology (such as material temperature limitations) and, if not, what thermodynamic requirements should be relaxed or what new technologies should be placed in the engine program in order to meet the system-level aircraft requirements. This study focused on developing (1) the structural and optimization methodology and the finite difference formulation for rotating disks, (2) a computer program to interface with the fluids and thermodynamic computer programs presently being used at NASA Lewis, and (3) a computer program to implement this desired structural and optimization methodology.

To verify the analytical results obtained from this study, the rotating disk of the 10th-stage compressor of the E^3 engine was modeled by using the finite element technique. The differences in the stress and displacement results from the computer program developed for this study and from the finite element technique were all less than 3%. The structural optimization results for a selective number of the rotating disks of the E^3 high-pressure compressor are also reported and compared with the flowpath analysis program WATE output and the E^3 drawings.

A pioneer in developing and documenting the methodology and structural formulation for rotating disks is Manson (ref. 1). Manson along with Millenson (ref. 2) and Mendelson (ref. 3) also pioneered the field of plasticity and low-cycle fatigue, and they tested and verified their structural methodology with structural experiments. The methodology developed by Manson

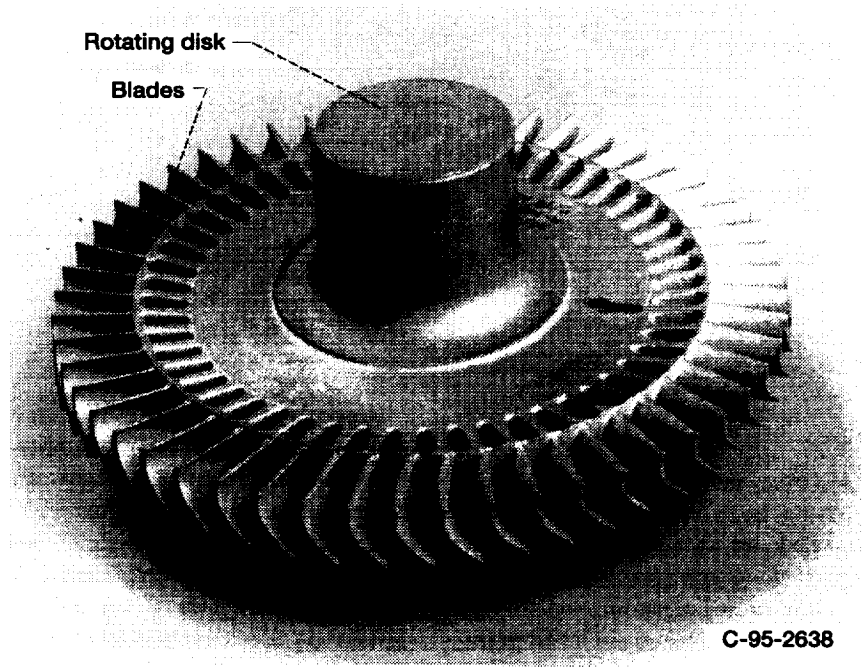

Figure 1.—Rotating disk and blades.

led to the finite difference technique, which was used here to solve the equilibrium and compatibility equations. One significant difference from Manson's methodology was that in this study disk thickness was a linear function of disk radius. In Manson's methodology disk thickness is constant. Furthermore, in this study the temperature gradients were also linear functions of disk radius. With linear assumptions for both temperature gradient and thickness variation, larger finite difference nodes could be used to predict the same stress, strain, and displacement levels for the same accuracy. Using larger finite difference nodes reduced the sizes of the matrices in the computer program and greatly shortened computation time. Short computation time was desirable in the present study because an optimization technique was used to predict the optimum weight while considering all the structural and design constraints. The computer program developed by Manson was written in 1947, and no attempt was made to obtain this program.

The methodology developed by Manson in reference 4, which predicts the low-cycle fatigue life of structural material, was closely followed in this study. The formulation of Manson's methodology is fully discussed in the section Low-Cycle Fatigue Methodology.

Symbols

A	disk cross-sectional area
D	material ductility
E	modulus of elasticity
F	force
J_p	polar mass moment of inertia
M	disk mass
m	slope in linear equation
N_f	low-cycle fatigue life in cycles
n	constant in linear equation; number of variables in minimization problem
q	number of constraint equations in minimization problem
r	radial distance to centroid of any differential element
r_g	radius of gyration
S_u	material ultimate strength
S_y	material yield strength
T	temperature difference between operating and assembly temperatures
t	disk thickness

u displacement in radial direction

W_{net} net work

α coefficient of thermal expansion

ε strain

θ rotational distance to centroid of any differential element

ν Poisson's ratio

ρ disk mass density

σ stress

ω rotational velocity

Subscripts:

avg average

i inside; node number

j disk section number

o outside

r radial

T temperature

z axial

θ rotational; tangential

Theory

The rotating disks of a gas turbine engine are subjected to body forces, blade loads, and thermal loads as well as shaft torque loads and engine thrust and landing loads. The important design loads are body forces, blade loads, and thermal loads. The influence of other loads on disk overall design is only local. The body forces and blade loads are proportional to the square of the rotational speed. The thermal loads are caused by the disk heating and cooling. Uneven heating and cooling cause a radial temperature gradient within the disks, in turn causing thermal loading. Thermal loads are linearly proportional to the radial temperature gradient.

The methodology and structural formulations in this study are based on the following assumptions:

(1) The thickness of the disk is small relative to its radius; thus (a) the variations of radial and tangential stresses over the thickness can be neglected (ref. 1), (b) the variation of temperature gradient in the axial direction can be neglected, and (c) a plane stress condition can be assumed.

(2) The displacements are small; thus the small-angle assumption can be made.

(3) The disk material is homogeneous and isotropic and follows Hook's law (ref. 5).

(4) The supporting structures for the rotating disks are flexible relative to the disk structure and do not impose a radial or tangential constraint on the disks. These supporting structures are thin cylinders and cones that connect the disks to each other and to the shaft. The only constraints that these cylinders and cones provide are in shear and torsion. The validity of this assumption was verified with the mechanical design group at General Electric Aircraft Engine Group (ref. 6).

Figure 2 shows a disk of variable cross section t whose inside radius is r_i and outside radius is r_o and a free-body diagram in the polar coordinate system of a differential element of the disk with all the applied loadings.

By using the preceding assumptions (1a), (1b), and (2), the sum of the loads in the radial and tangential directions can be expressed as

$$\sum F_\theta = 0 \tag{1}$$

$$\sum F_r = 0, \text{ which results in } \frac{dF_r}{dr}dr - F_\theta d\theta + \rho r^2 \omega^2 dr d\theta = 0 \tag{2}$$

where

F_θ force in tangential direction

F_r force in radial direction

r radial distance to centroid of any differential element

θ tangential distance to centroid of any differential element

ρ disk mass density

ω rotational velocity

In a biaxial stress state (assumption 1c), the stresses in the axial direction are zero. Therefore, the forces in the axial direction were not considered in this study. In terms of the

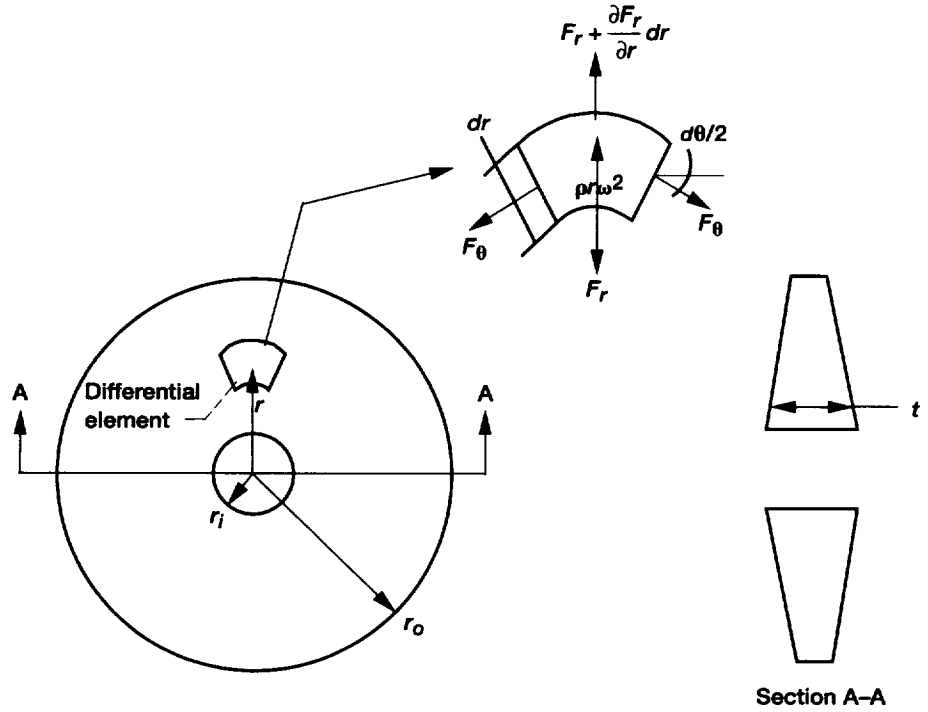

Figure 2.—Typical rotating disk.

stresses acting on the surfaces of the differential element

$$F_r = \sigma_r r t d\theta \tag{3}$$

$$F_\theta = \sigma_\theta t dr \tag{4}$$

where

σ_θ tangential component of stress

σ_r radial component of stress

The disk thickness as a linear function of the radial distance is

$$t = mr + n \tag{5}$$

where

m slope

n constant

Substituting equations (3) to (5) into equation (2) results in the equilibrium equation for the disk:

$$\frac{d\sigma_r}{dr} + \frac{2mr + n}{mr^2 + nr}\sigma_r - \frac{1}{r}\sigma_\theta + \rho r\omega^2 = 0 \tag{6}$$

The terms in equation (6) reveal an interdependency between the radial and tangential stresses. Next, this interdependency should be defined and substituted back into the equation in order to have only one variable. It may appear in equation (6) that there are mechanical loads only and no thermal loads. However, the influence of the thermal loads in the overall disk loading is included in the strain relationships and thus in the stress terms. By using assumptions (1b), (1c), and (3), the relationships between the stresses and strains in two orthogonal dimensions can be expressed as (ref. 5)

$$\varepsilon_r = \frac{1}{E}\left(\sigma_r - \nu\sigma_\theta\right) + \alpha T \tag{7}$$

$$\varepsilon_\theta = \frac{1}{E}\left(\sigma_\theta - \nu\sigma_r\right) + \alpha T \tag{8}$$

where

ε_r radial component of strain

ε_θ tangential component of strain

E modulus of elasticity

ν Poisson's ratio

α coefficient of thermal expansion

T temperature difference between operating and assembly temperatures

Equations (7) and (8) are solved for the stresses in the radial and tangential directions to obtain

$$\sigma_r = \frac{E}{1-\nu^2}\left[\varepsilon_r + \nu\varepsilon_\theta - (1+\nu)\alpha T\right] \tag{9}$$

$$\sigma_\theta = \frac{E}{1-\nu^2}\left[\varepsilon_\theta + \nu\varepsilon_r - (1+\nu)\alpha T\right] \tag{10}$$

The strains in the polar coordinate system are defined as (ref. 5)

$$\varepsilon_\theta = \frac{u}{r} \tag{11}$$

$$\varepsilon_r = \frac{du}{dr} \tag{12}$$

where

u displacement in radial direction

Equations (11) and (12) suggest that all the variables sought in this study, such as the stresses and strains, are functions of only the radial displacement. Substituting equations (11) and (12) into (9) and (10) results in

$$\sigma_r = \frac{E}{1-\nu^2}\left[\frac{u}{r} + \nu\frac{du}{dr} - (1+\nu)\alpha T\right] \tag{13}$$

$$\sigma_\theta = \frac{E}{1-\nu^2}\left[\frac{du}{dr} + \nu\frac{u}{r} - (1+\nu)\alpha T\right] \tag{14}$$

Differentiating equation (13) with respect to radius and substituting it along with equations (13) and (14) into equation (6) result in a single differential equation with one variable, displacement:

$$\frac{d^2u}{dr^2} + \left(\frac{2mr+n}{mr^2+nr}\right)\frac{du}{dr} + \left[\frac{\nu}{r^2} - \frac{1}{r^2} + \frac{\nu}{r}\left(\frac{2mr+n}{mr^2+nr}\right)\right]u =$$

$$\alpha(1+\nu)\left[\frac{dT}{dr} + \left(\frac{2mr+n}{mr^2+nr} - 1\right)T\right] - \frac{\rho\omega^2\left(1-\nu^2\right)}{E}r \tag{15}$$

Equation (15) represents the disk displacement field and is a boundary value problem. The difference between equation (15) and what has been reported in the literature reviewed in this study is that equation (15) includes linear relationships for the thickness and temperature distribution as functions of the radius. These additional capabilities enable the analyst to more accurately predict the stresses and displacements with fewer finite difference nodes. Equation (15) is a linear, second-order, nonhomogeneous differential equation with variable coefficients and requires two boundary condition equations for a complete and quantitative solution. The boundary conditions that lead to the solution for this equation can be derived from the physical environment at the disk bore and rim. At the bore the radial stress is zero. At the rim the radial stress is equal to the centrifugal loads resulting from the rotation of the blades and their support points divided by the cross section of these support points.

In the preceding discussion, since no additional constraints (boundary conditions) were imposed on the disks, the rotating disks may appear to be freely floating. In reality, these disks are not freely floating and cannot possess any rigid-body motions. The disks not only support the blades, they also provide the load paths for transferring the torque from the shaft to each other and for transferring shear and bending of the rotor subassembly. The disks are free at the bore; that is, there is no connection between the disks and the shaft so that the required cooling air can freely flow through the disks. The disks are connected at the rim to each other and to the shaft through a series of thin cylinders and cones. As explained in assumption (4), the relatively thin cones and cylinders do not impose a high level of structural constraint on the disks. Relative to their supporting thin cylinders and cones, the disks are structurally massive and stiff. Therefore, the cylinders and cones will deform rather freely when the disks are under thermal and/or centrifugal loadings. As a result, in this study, no outside constraints from the supporting structures are imposed on the disks. The boundary condition equations can be expressed as

$$\sigma_{r=r_i} = 0; \quad \text{thus,} \quad \frac{u}{r} + \nu\frac{du}{dr} - (1+\nu)\alpha T = 0 \tag{16}$$

$$\sigma_{r=r_o} = \sigma_{\text{blade}}; \quad \text{thus,} \quad \frac{u}{r} + \nu\frac{du}{dr} - \frac{\sigma_{\text{blade}}E}{1-\nu^2}$$

$$-(1+\nu)\alpha T = 0 \qquad (17)$$

Equations (16) and (17) are also nonhomogeneous differential equations.

General Solution, Finite Difference Approach

There are many methods in the literature for solving equation (15) along with its boundary conditions, equations (16) and (17). Some of these methods are superposition, chasing, adjoint operator, shooting, and transformation (ref. 7). However, these methods are only appropriate for a continuum with a one-time variation in the coefficients of the equation. When considering a practical rotating disk, the disk thickness varies with radius at least five times (fig. 3).

Equation (15) should satisfy the displacements and stresses of all disk sections, 1 to 5, at the same time. The appropriate method for solving equation (15) is either the finite element method or the finite difference method. The finite element method was not used in this study because, in general, it consumes more computer time due to operating on larger matrices. Computer time becomes a significant issue when an optimization technique is used to arrive at an optimum solution. In this study an optimization technique was used to determine the sizes of the rotating disks. Therefore, the finite difference technique was used to solve equation (15) along with its boundary conditions, equations (16) and (17).

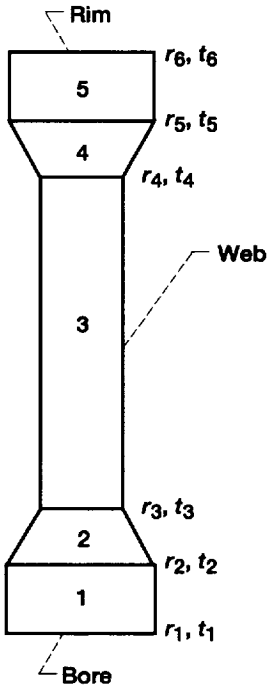

Figure 3.—Schematic of disk cross section, where r_i is the radius of section i and t_i is the thickness of section i (i = 1 to 6).

Next, equations (15) to (17) were transformed into the finite difference format. Equations (15) to (17) have two terms that contain the first and the second derivatives of displacement with respect to radius. By employing the Taylor series to expand the first derivative of displacement with respect to radius and selecting only two terms as an approximation, the first derivative can be expressed as (ref. 7)

$$\frac{du}{dr} = \frac{u_{i+1} - u_i}{\Delta r} + O(\Delta r) \qquad (18)$$

where

u_i displacement of node i

Δr difference between radii of node (i+1) and node i

$O(\Delta r)$ first-degree errors due to truncation

The second derivative of displacement with respect to radius can be expressed as (ref. 7)

$$\frac{d^2u}{dr^2} = \frac{u_{i-1} - 2u_i + u_{i+1}}{\Delta r} + O(\Delta r) \qquad (19)$$

Substituting equations (18) and (19) into (15) results in an equation representing the displacement field for the internal nodes of the disks, as follows:

$$\frac{1}{\Delta r_i^2}u_{i-1} - \left[\frac{2}{\Delta r_i^2} + \frac{2mr_i + n}{\Delta r_i\left(mr_i^2 + nr_i\right)} + \frac{\nu mr_i - m\nu - n}{mr_i^3 + nr_i^2}\right]u_i$$

$$+\left[\frac{1}{\Delta r_i^2} + \frac{2mr_i + n}{\Delta r_i\left(mr_i^2 + nr_i\right)}\right]u_{i+1} = -\frac{\left(1-\nu^2\right)\rho\omega^2}{E}r_i$$

$$+(1+\nu)\alpha\left[\frac{m(m_T r_i + n_T)}{mr_i + n} + m_T\right] \qquad (20)$$

where

m_T slope of temperature gradient with respect to radius in linear equation $T_i = m_T r_i + n_T$

n_T constant in linear equation $T_i = m_T r_i + n_T$

The approach taken to derive the finite difference equation for the boundary conditions was somewhat different from the one used in equation (20). Although the approach could have been the same, due to the anticipated high stress gradients at the disk bore and rim, the finite difference equations for the first derivatives were modified and improved to provide higher accuracy. In this approach the first derivatives of displacement with respect to radius are contained in three terms. To derive the three-term, first-derivative equation, the Taylor series about point i can be expanded as

$$u_{i\pm1} = u_i \pm \left(\frac{du}{dr}\right)_i \Delta r + \frac{1}{2}\left(\frac{d^2u}{dr^2}\right)_i \Delta r^2 \pm \frac{1}{6}\left(\frac{d^3u}{dr^3}\right)_i \Delta r^3 + O(\Delta r)^4 \qquad (21)$$

$$u_{i\pm2} = u_i \pm \left(\frac{du}{dr}\right)_i 2\Delta r + \frac{1}{2}\left(\frac{d^2u}{dr^2}\right)_i 4\Delta r^2 \pm \frac{1}{6}\left(\frac{d^3u}{dr^3}\right)_i 8\Delta r^3 + O(\Delta r)^4 \qquad (22)$$

where

$O(\Delta r)^4$ fourth-order errors due to truncation

Multiplying equation (21) by 4 and subtracting equation (22) result in

$$\frac{du}{dr} = \pm\frac{-3u_i + 4u_{i\pm1} - u_{i\pm2}}{2\Delta r} + O(\Delta r)^2 \qquad (23)$$

where

$O(\Delta r)^2$ second-order errors due to truncation

Substituting equation (23) into equations (16) and (17) results in the finite difference equations for the boundaries of the disk at its bore and rim:

$$\left(-\frac{3}{2\Delta r} + \frac{\nu}{r}\right)u_i + \frac{2}{\Delta r}u_{i+1} - \frac{1}{2\Delta r}u_{i+2} = (1+\nu)\alpha T_i \qquad (24)$$

$$\left(\frac{3}{2\Delta r} + \frac{\nu}{r}\right)u_i - \frac{2}{\Delta r}u_{i-1} + \frac{1}{2\Delta r}u_{i-2} = \frac{1-\nu^2}{E}\sigma_{\text{blade}} + (1+\nu)\alpha T_i \qquad (25)$$

Equations (20), (24), and (25) provide the complete solution for a rotating disk whose thickness and temperature are linear functions of the disk radius. The external mechanical loads are provided through the stresses at the rim, and these stresses are calculated from the centrifugal blade loads acting on the rim. The thermal loads are the radial temperatures of the disk. In each of the five disk sections of figure 3 the thickness varies differently with radius. The temperature distribution in each section also varies differently with radius. Therefore, at the boundaries joining the disk sections the appropriate compatibility equations should be derived and transformed into the finite difference format.

At the boundaries joining adjacent sections of the disk the displacements and stresses of one section should be equal to those of the adjoining section. The compatibility equations for the stress and displacement are as follows:

$$\sigma_{r_j} = \sigma_{r_{j+1}} \qquad (26)$$

$$\sigma_{\theta_j} = \sigma_{\theta_{j+1}} \qquad (27)$$

$$u_j = u_{j+1} \qquad (28)$$

where

j subscript denoting disk section number

Note that because nodes j and j+1 do not have the same radial dimensions, equations (26) to (28) are only approximations. By using the definitions of the radial and tangential stresses in equations (13) and (14), equations (26) and (27) can be rewritten as

$$\left[\frac{u}{r} + \nu\frac{du}{dr} - (1+\nu)\alpha T\right]_j = \left[\frac{u}{r} + \nu\frac{du}{dr} - (1+\nu)\alpha T\right]_{j+1} \qquad (29)$$

$$\left[\frac{du}{dr} + \nu\frac{u}{r} - (1+\nu)\alpha T\right]_j = \left[\frac{du}{dr} + \nu\frac{u}{r} - (1+\nu)\alpha T\right]_{j+1} \qquad (30)$$

Substituting equation (28) into equations (29) and (30) and subtracting the result in the compatibility equation for the slope of displacement:

$$\left(\frac{du}{dr}\right)_j = \left(\frac{du}{dr}\right)_{j+1} \tag{31}$$

Therefore, if the requirements of equations (29) and (30) at the boundaries between adjacent sections of the disk are met, the requirements for the stresses and other important elasticity variables will be satisfied as well. Substituting equation (23) into (31) results in the finite difference equations for the boundaries between adjacent sections of the disk:

$$u_i = u_{i+1} \tag{32}$$

$$\frac{+3u_i - 4u_{i-1} + u_{i-2}}{2\Delta r_j} = \frac{-3u_{i+1} + 4u_{i+2} - u_{i+3}}{2\Delta r_{j+1}} \tag{33}$$

The radial increments may be different in each disk section, and equation (33) takes this fact into account. The compatibility equation (33) is more accurate than the two-term finite difference equation, since the truncated errors are of higher magnitude. With the anticipated accuracy that equation (33) offers, the increments for the nodalization at the boundaries between two adjacent sections do not have to be as small as when a two-term finite difference equation for the slope is used. Larger finite difference nodes reduce the sizes of the analytical matrices, resulting in shorter computation time.

An important stress value used in designing rotating disks is the average tangential stress. This stress should meet the requirements stated in the section Structural Design Requirements. The average tangential stress is calculated for the case where the rotating disk yields, diminishing the radial stiffness and the thermally induced loads. One method for predicting this stress is to determine the net tangential force (by multiplying the tangential stresses due to the mechanical and body forces by their respective areas), and divide this force by the disk cross section area. Another method for predicting such a stress is simply to divide the net centrifugal loads of the entire rotating disk and the blades by the disk cross-sectional area. The following steps were taken to determine the average tangential stress (note that the following equation can easily be derived by using the basic geometry and static theory):

(1) Calculate the cross-sectional area of the rotating disk by using

$$A = 2\sum_{j=1}^{j=5}\left[\frac{m_j}{2}\left(r_o^2 - r_i^2\right) + n_j\left(r_o - r_i\right)\right] \tag{34}$$

(2) Calculate the mass of the rotating disk and the blades by using

$$M = 2\pi\rho\sum_{j=1}^{j=5}\left[\frac{m_j}{3}\left(r_o^3 - r_i^3\right) + \frac{n_j}{2}\left(r_o^2 - r_i^2\right)\right] + M_{\text{blade}} \tag{35}$$

(3) Calculate the polar mass moment of inertia of the rotating disk and the blades by using

$$J_p = 2\pi\rho\sum_{j=1}^{j=5}\left[\frac{m_j}{5}\left(r_o^5 - r_i^5\right) + \frac{n_j}{4}\left(r_o^4 - r_i^4\right)\right] + M_{\text{blade}} r_{\text{c.g.}}^2 \tag{36}$$

(4) Calculate the radius of gyration of the rotating disk and the blades by using

$$r_g = \sqrt{\frac{J_p}{M}} \tag{37}$$

(5) Calculate the tangential force acting on the rotating disk by using

$$F_\theta = M r_g \omega^2 \tag{38}$$

(6) Calculate the average tangential stress in the rotating disk by using

$$\sigma_{\theta,\text{avg}} = \frac{F_\theta}{A} \tag{39}$$

Loads Methodology

As previously stated, several types of loads act on the rotating disks. Mechanical loads are either internal or external. The internal loads, which are due to the body forces of the disk material, have already been included in the equilibrium and compatibility equations. The external loads, which are used to design the rotating disks, are caused by the centrifugal loads on the blades and their support points (fig. 4). Section 6 of this figure shows the entire blade support points. These support points consist of airfoil, platform, dovetail, and the sections of the rotating disk between the dovetail slots.

The slots into which the blade dovetail slides cause a stress discontinuity in the tangential direction. This discontinuity also causes the tangential stiffness of the rotating disk to be zero; thus, the tangential stresses are zero. As a result, all the centrifugal loads are reacted in the radial direction at the boundary between sections 5 and 6. Therefore, in this study the centrifugal loads caused by blade rotation and section 6 were

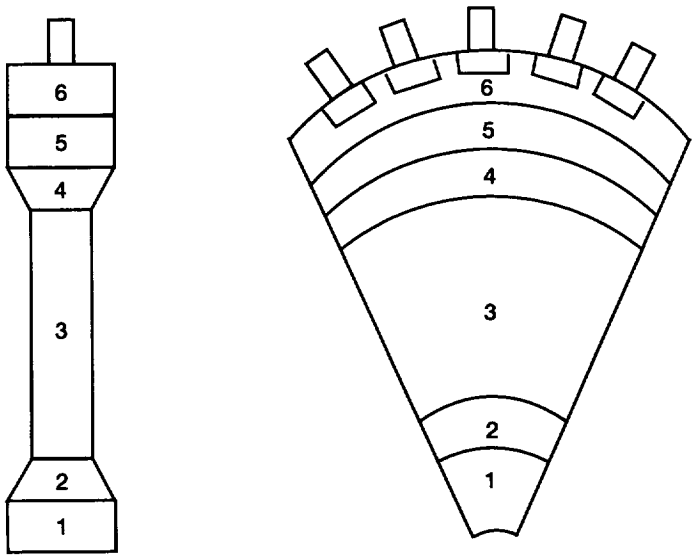

Figure 4.—Schematics of disk cross section and disk sector.

calculated and summed. The total load was then applied as an external load to section 5. The finite difference model, therefore, includes only sections 1 to 5.

To determine the centrifugal loads on the blade airfoil, the following steps were taken:

(1) The blade height was calculated as the difference between the outside and inside radii of the flowpath. These radii were available in the output for each stage of the compressor or the turbine from the engine flowpath analysis.

(2) The chord length of the blade is equal to its height divided by its aspect ratio. The blade aspect ratio is available in the output for each stage of the compressor or the turbine from the engine flowpath analysis.

(3) A volume containing the blade was calculated as the blade height multiplied by the area formed from a square with sides equal to the blade chord length.

(4) The volume of the blade airfoil was approximated by multiplying a volume factor by the volume calculated in step (3). The volume factors were 0.024 for the high-pressure fan blade, 0.199 for the fan blade, 0.047 for the low-pressure compressor, and 0.163 for the high-pressure compressor (ref. 8).

(5) The mass of the blade airfoil is then its volume times its mass density. See the section Material Data Base for a discussion of material properties, such as density, for various stages of the compressor and the turbine.

(6) The centrifugal load of the blade airfoil was calculated by multiplying the airfoil's mass by its center of gravity from the centerline of rotation.

(7) The load from a single airfoil was multiplied by the number of blades at each stage of the compressor or the turbine to obtain the total blade load. The number of blades is available in the output for each stage of the compressor or the turbine from the engine flowpath analysis.

The centrifugal loads caused in section 6 were computed by assuming it to be a rotating ring. Finally, the total centrifugal loads on the blade airfoils and section 6 were applied at the outer radius of section 5.

The thermal loads are essentially caused by the temperature differences between the adjacent finite difference nodes. This temperature distribution needs to be predicted by using other computer programs that can perform thermal analysis of axisymmetric continua.

Low-Cycle Fatigue Methodology

The methodology used for predicting low-cycle fatigue life was based on work by Manson (ref. 4). Manson used the method of universal slopes to represent the fatigue properties of 29 materials in terms of their elastic and strength properties. The material data base includes materials with crystalline structures having body-centered-cubic, face-centered-cubic, and hexagonal-close-packed arrangements. Other variables considered in Manson's material data base are reductions in area from 1 to 94%, tensile strengths from 16 000 to 400 000 psi, high and low notch sensitivities, cyclic hardening and softening characteristics, and high and low stacking faults. The low-cycle fatigue equation based on Manson's work is

$$\Delta\varepsilon = 3.5\frac{S_u}{E}N_f^{-0.12} + D^{0.6}N_f^{-0.6} \tag{40}$$

where

$\Delta\varepsilon$ strain range

S_u material ultimate strength

N_f low-cycle fatigue life in cycles

D material ductility

Equation (40) is based on the actual separation of the test specimen, and the exponent of –0.6 is indicative of this fact. In an earlier investigation by Coffin (ref. 9) the exponent of the cyclic life was suggested to be –0.5. The work by Coffin is also based on extensive fatigue testing of material. However, Coffin's failure criterion is different from the one selected by Manson. Coffin's failure criterion is the initial cracking of the test specimen. In fact, he regarded the test complete if he observed the first visual cracking. In this study Manson's methodology was used, although it may seem less conservative. The reasons for selecting a less conservative approach are (1) this study should be extended to include elastic-plastic analysis and the fatigue equation should cover the plastic region, (2) a safety factor of 4.0 was used to reduce the predicted life per equation (40), minimizing the effects of any uncertainties, and (3) Manson used a larger material data base than did Coffin, making Manson's equation more universal.

The strain range in equation (40) is for a specimen loaded in only the axial direction. The disk material was loaded in two directions, radial and tangential. Therefore, a strain value representative of all loads in all directions should be used in this equation. Mendelson suggests using the equivalent strain range in equation (40) (ref. 3). The equivalent strain range is based on the maximum-distortion-energy theory (ref. 10) and has the following form:

$$\Delta\varepsilon = \frac{\sqrt{2}}{3}\sqrt{(\varepsilon_r - \varepsilon_\theta)^2 + (\varepsilon_\theta - \varepsilon_z)^2 + (\varepsilon_r - \varepsilon_z)^2} \quad (41)$$

where the subscripts show the strain directions.

The strain in the z direction was obtained by using the plane stress theory. For a biaxial stress state (the axial stress was assumed to be zero), the equation for the axial strain can be expressed as

$$\varepsilon_z = -\frac{\nu}{E}(\sigma_r + \sigma_\theta) \quad (42)$$

In summary, after the calculations of displacements the steps taken to predict low-cycle fatigue life were as follows:

(1) Determine the strains by using equations (12), (13), and (42)

(2) Determine the equivalent strain range by using equation (41)

(3) Substitute the equivalent strain range into equation (40) and solve for the low-cycle fatigue life

Material Data Base

A material data base was developed and included in the computer program used in this study. A primary objective in developing this methodology was to provide an opportunity for engineers with varying backgrounds to successfully use it. Two materials widely used in aircraft engines have been included in the material data base. These materials are Inconel-718 and titanium–6 wt% aluminum–4 wt% vanadium (Ti-6Al-4V). The elastic, thermal, and strength properties of Inconel-718 and Ti-6Al-4V at room temperature were obtained from references 11 and 12, respectively. In this methodology the rotating disk and the blades are selected as Ti-6Al-4V so long as the flowpath stagnation temperature is 1200 °F or less. At temperatures above 1200 °F the materials of the rotating disk and the blades switch to Inconel-718. The material data base should be expanded to include more superalloys and to make the properties temperature dependent.

Structural Design Requirements

The structural design requirements were gathered from references 13 and 14. The objective of acquiring and implementing these design requirements is to enable users to conceptually design the rotating disks within the acceptable known limits of design practices followed by both NASA and industry. These requirements have been implemented in the computer program such that stress, low-cycle fatigue life, safety margin, and other output information need not be modified with any additional safety factors. The requirements are as follows:

(1) The safety factors based on yield strength and ultimate strength are 1.1 and 1.5, respectively (ref. 13). The strength properties obtained from the material data base are decreased by these safety factors.

(2) The number of cycles to failure should be four times the number of predicted operating cycles for low-cycle fatigue (ref. 13).

(3) The maximum operating speed should be set 5 to 10% higher than the expected maximum compressor or turbine speed (ref. 13). In this study an overspeed percentage of 15% (ref. 14) was used.

(4) Disk-web-combined primary and secondary effective stress should be less than the yield strength (ref. 13).

(5) Disk-bore-combined primary and secondary effective stress should also be less than the yield strength.

(6) Disk-average primary tangential stress at 120% speed should be less than 90% of the ultimate strength (ref. 14). This

particular design requirement is established based on the assumption that the disk has already yielded, the thermal stresses have been redistributed and thus diminished, disk radial stiffness has completely diminished, and the disk can only react to the mechanical loads in the tangential direction. This requirement is conservative but important to use, since in case of yielding, disk failure should be prevented. The rotating disks possess large amounts of kinetic energy, and in case of failure, which means separation of the rotating disk, there is not enough containment shield to contain the failed pieces. Because the weight considerations and the aerodynamic design make the use of such containment shields impractical, rotating disks should be designed conservatively enough to eliminate the need for such containment shields.

(7) The rotating disks should be designed by using material properties for the maximum temperature environment.

Optimization Methodology

Success in a structural analysis is measured by providing positive, but near zero, structural margins of safety for the user. For this purpose an existing optimization technique was used. The optimization technique modifies and improves the rotating disks if they have negative margins of safety, and saves time for the user. The time saved by using an optimization technique in this study was tremendous, since the iterations that must be done manually by the user are done automatically by the computer. This time saving can be as high as approximately two to three weeks per rotating disk. No more than 5 min of elapsed time was consumed by the computer for the structural optimization of the rotating disks.

The optimization technique selected for this study was the sequence of unconstrained minimizations technique (SUMT). This technique is widely used for solving linear and nonlinear constraints or unconstrained function minimization problems. The problem must be formulated as follows:

$$\text{Minimize} \quad F(x_1, x_2, \ldots, x_n) \tag{43}$$

$$\text{Subject to} \quad g_q(x_1, x_2, \ldots, x_n) \geq 0 \qquad q = 1, 2, \ldots, Q \tag{44}$$

where

$F(x_1, x_2, \ldots, x_n)$	objective functions
$g_q(x_1, x_2, \ldots, x_n)$	constraint functions
$x_1, x_2, \ldots, x_n$	variables to be determined
n	number of variables
Q	number of constraint equations

In this study the objective function to be minimized was disk mass as obtained per equation (35). The design variables were r_1, t_1, r_2, r_3, t_3, and r_4. In a practical rotating disk t_2 and t_4 are equal to t_1 and t_3, respectively. The remainder of the dimensions (i.e., r_5, t_5, r_6, and t_6) were known.

The constraint equations were defined as follows:

$$r_2 - r_1 > 0$$

$$r_3 - r_2 > 0$$

$$r_4 - r_3 > 0$$

$$r_5 - r_4 > 0$$

$$\text{Stresses at bore, web, rim} < \frac{S_y}{1.1}$$

$$\text{Average tangential stress at 120\% speed} < 0.9S_u$$

The constraint equations related to the radii and thicknesses were based on observation of the overall sizes of the E^3 engine's rotating disks. The constraint equations related to the strength properties, however, were based on the design requirements. Finally, the constraint equation related to the life of the rotating disk was based on the design requirements and reference 14. The computer program used for the optimization was NEWSUMT (ref. 15).

The optimization process was as follows:

(1) A rotating disk was given an initial geometry based on the radii of the shaft and the flowpath and the chord length of the blade.

(2) Given the geometry and loads calculated, the constraints of the problem were evaluated.

(3) Upon violation of any of the constraints the disk geometry was modified until the conditions for all constraint equations were met and the weight was a minimum.

Description of Computer Program

A FORTRAN computer program was developed for this study. The overall flow of this computer program is shown in figure 5. The computer program was designed to generate the geometry and the mechanical loads of each rotating disk and then proceed with the structural optimization analysis. The user must input the thermal loads into the computer program through the coefficients of a polynomial representing the radial

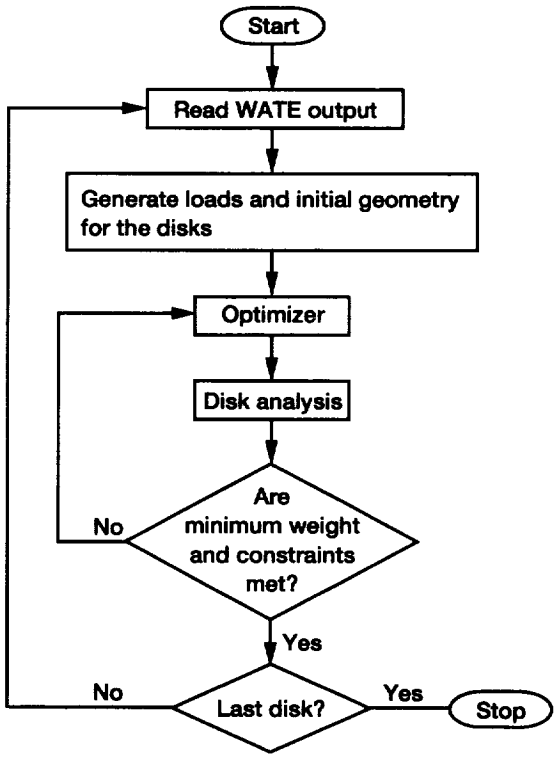

Figure 5.—Block diagram of computer program developed for this study.

temperature profile of the rotating disk. Up to a fifth-degree polynomial can be used. If the coefficients are not input, the program sets the thermal loads equal to zero.

Verification

The stress analysis portion of the computer program developed for this study was verified in two steps. First, a constant-thickness, mechanically loaded rotating disk was employed for verification. Next, the 10th-stage, high-pressure-compressor rotating disk of the E^3 engine, which has complex geometry and loading, was used to complete the verification. Then, the entire computer program was used to structurally optimize two rotating disks of the E^3 high-pressure compressor.

When verifying the computer program developed for this study by using a constant-thickness rotating disk, three methods were used to calculate the stresses and displacements. The reason for using three methods was not only to verify the finite difference technique and the methodology in this study, but also to determine the accuracy of a finite element technique that would be used later to verify a more complex rotating disk. The methodology of reference 16 was used to analytically model a constant-thickness rotating disk. The loads acting on the constant-thickness rotating disk were only centrifugal owing to the capability of the method in reference 16. Then, the stresses and displacements were calculated. Next, the computer program developed for this study was used to model the constant-thickness rotating disk, and the resulting stresses and displacements were also calculated. Finally, a finite element technique, the MSC/NASTRAN computer program, was used to model the constant-thickness rotating disk, and the resulting stresses and displacements were recovered (ref. 17). The respective differences between the stresses and displacements among the three methods were all less than 5%. The results of this verification showed that the computer program and the methodology in this study are accurate for a simple-geometry disk. Other useful information obtained in this step was that the MSC/NASTRAN computer program is accurate enough to be used as a verification tool for complex-geometry rotating disks.

When verifying a computer program, the program should be supplied with the most stringent input in order to determine its capabilities and limitations. In the case of the computer program developed for this study, the most stringent test would be to use a complex-geometry rotating disk acted on by a combination of thermal and mechanical loads. Therefore, the E^3 engine was used for this portion of the verification. To complete the verification, the 10th-stage rotating disk of the E^3 engine's high-pressure compressor was modeled by using both MSC/NASTRAN and the finite difference technique of this study. Since accurate radial temperature distributions for the E^3 rotating disks were not available and the objective here was only to verify the methodology, a typical radial distribution for a rotating disk was assumed (ref. 2).

Figure 6 shows a fringe plot of the Von Mises stresses in the finite element model of the 10th-stage rotating disk of the E^3 engine's high-pressure compressor. As expected, the stresses around the bore area (red area of fig. 6) were highest since this area was essentially the foundation and thus the main load-bearing section of the structure. The stresses around the rim area (blue area of fig. 6) were lowest. As the radius decreased, the stresses increased—blue changed to red—meaning the loads increased as the radius decreased. The reason for this load increase was that the structural material at lower radii carried the radial loads induced by the material at higher radii. This argument can be true as long as the temperature gradients at higher radii are not too much higher than the ones at lower radii. The results of this verification have been tabulated in table I.

The 10th-stage rotating disk of the E^3 engine was modeled per its drawing dimensions and was not optimized for weight in this verification process because the NEWSUMT subroutine is verified in reference 15.

The final verification step was to structurally optimize the rotating disks of an engine. The objective of this optimization was to subjectively examine the methodology and the computer program by determining whether the results (i.e., dimensions and weights) were meaningful. Since the layout drawings of the E^3 engine and its operating conditions were available, the computer program developed for this study was used to examine the rotating disks of this engine's high-pressure compressor.

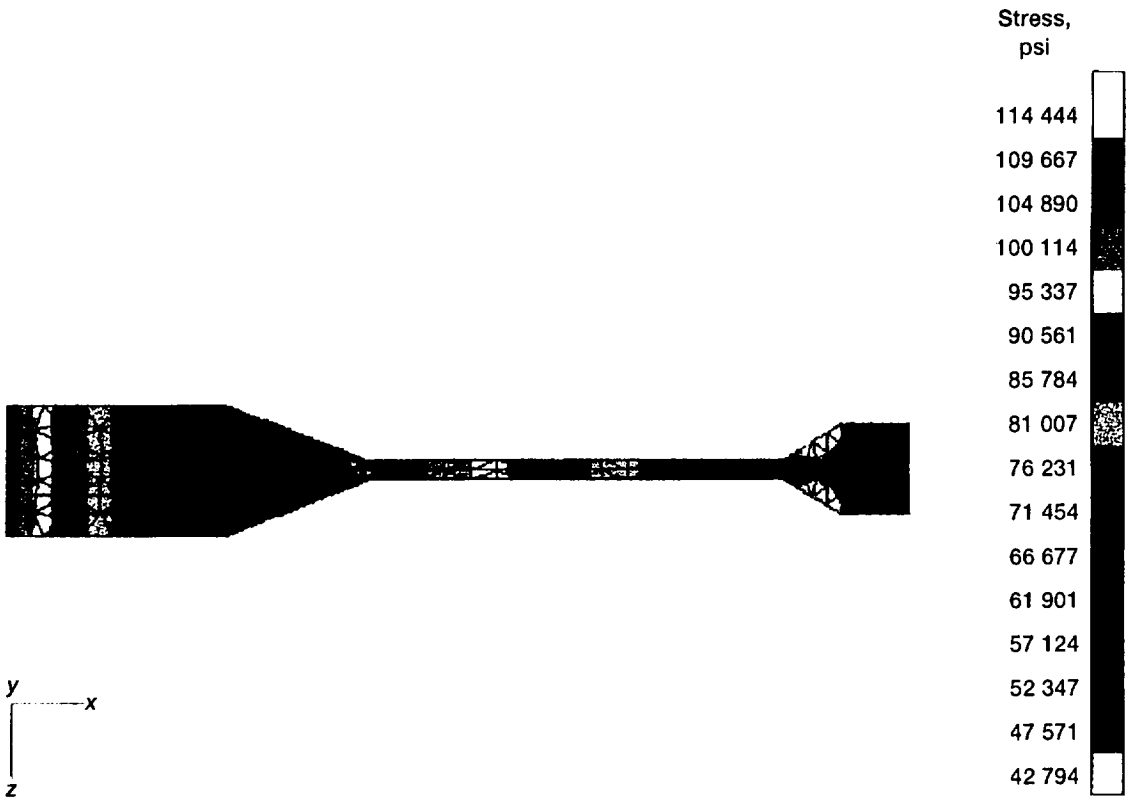

Figure 6.—Fringe plot of von Mises stress for 10th-stage rotating disk of E^3 high-pressure compressor.

TABLE I.—RESULTS OF VERIFICATION USING 10TH-STAGE DISK OF E^3 ENGINE

Parameter	MSC/NASTRAN	Finite difference	Difference, percent
Bore stress, psi	106 175	109 667	3.2
Rim displacement, in.	0.038065	0.038869	2.1

The objective of this examination was only to see how close the dimensions and weights obtained from this computer program were to those obtained from the E^3 drawings and the WATE computer output. One of the design drivers of the rotating disks is the radial thermal gradients within the disks, and for the E^3 engine these data were not available. Therefore, only the rotating disks of the second and third stages of the high-pressure compressor were structurally optimized. The gas temperatures at these lower stages of the compressor are still low enough (approximately 600 °F for the second stage and 800 °F for the third stage) that the thermal loads can be neglected. The results of this optimization are summarized in tables II and III and figures 7 and 8.

Figures 7(a) and 8(a) show the dimensions of the second-stage and third-stage rotating disks as obtained from the computer program developed for this study. Figures 7(b) and 8(b) show the dimensions of the second-stage and third-stage rotating disks per the E^3 drawings. The E^3 disks were redrawn to visually determine whether the overall dimensions obtained by the methodology in this study sensibly compared with the dimensions of actual hardware. Examining figures 7 and 8 reveals that the methodology in this study tended to extend the disks in the radial direction and that in the process the webs were thinned. Extending the disk and thinning the web makes sense mathematically and physically. Mathematically, when the structural mass of the disk is located near its centerline, the disk will weigh less; thus, the disks should be stretched toward the centerline. Physically, the structural mass near the centerline can offer higher tangential stiffness and strength; thus, the structural mass of the disk should be stretched toward the centerline.

Examining the values in tables II and III reveals that the masses calculated by the computer program were lower than the masses obtained from the E^3 drawings. This finding was discussed with General Electric, and the explanation was that since the E^3 engine was not flight hardware, no attempts had been made to minimize its weight (ref. 18). Therefore, the E^3 disk weights are somewhat higher than what they might have been for a flight engine.

In an effort to gain a general knowledge of the time consumed by the central processing unit (CPU), the computer program developed for this study was tested on a VAX–9000

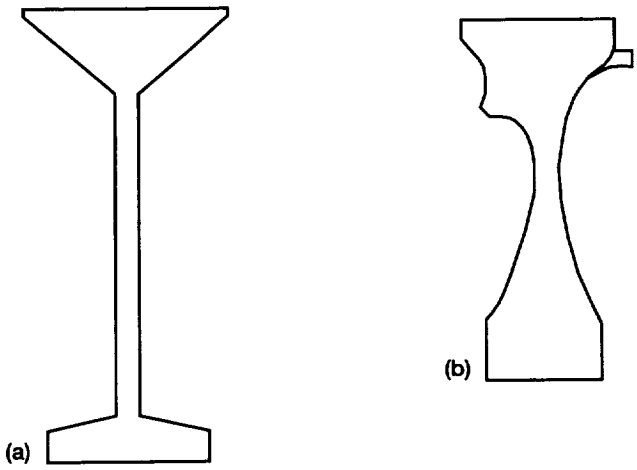

Figure 7.—Second-stage rotating disk of E^3 high-pressure compressor. (a) Design optimization program code. (b) E^3 drawing.

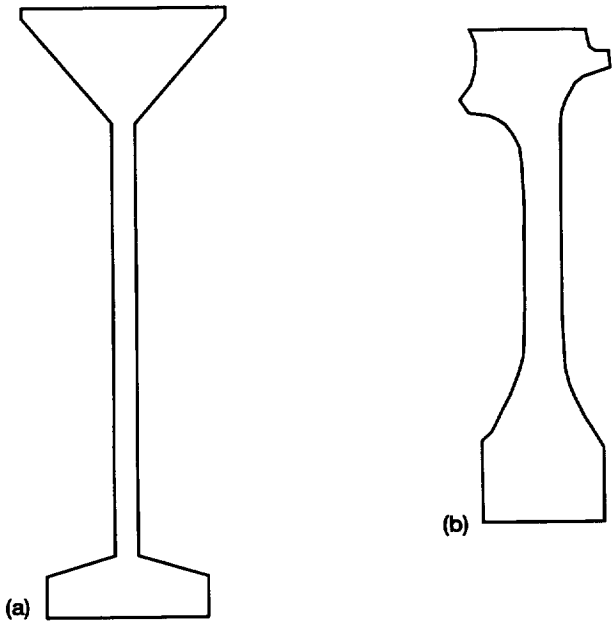

Figure 8.—Third-stage rotating disk of E^3 high-pressure compressor. (a) Design optimization program code. (b) E^3 drawing.

and again on an IBM–RISC6000 computer. The WATE output for the E^3 engine was used for these two tests, and the objective was to structurally optimize the high-pressure-compressor rotating disks. The structural optimization of 10 rotating disks of the E^3 engine's high-pressure compressor consumed 20 min of CPU time on a VAX–9000 computer and 30 min of CPU time on an IBM–RISC6000 computer. No firm conclusion, however, can be drawn from this CPU time consumption study, since the structural optimization of 10 rotating disks of the

TABLE II.—RESULTS OF STRUCTURAL OPTIMIZATION OF SECOND-STAGE DISK OF E^3 HIGH-PRESSURE COMPRESSOR

Parameter	Method			Maximum difference, percent
	E^3 drawing	WATE	Finite difference	
Weight, lb	56.8	59	49.3	16.4
Material	Ti-6Al-4V	Ti-6Al-4V	Ti-6Al-4V	(b)
Life, cycles	(a)	(a)	190 000	
Average safety margin	(a)		0.06	
Safety margin	(a)		0.02	
r_1, in.	4.30		3.54	
$t_2 = t_1$, in.	1.25		1.74	
r_2, in.	4.85		3.67	
r_3, in.	6.10		4.24	
$t_4 = t_3$, in.	0.25		0.12	
r_4, in.	7.80		7.41	

[a]Not provided.
[b]Not applicable.

TABLE III.—RESULTS OF STRUCTURAL OPTIMIZATION OF THIRD-STAGE DISK OF E^3 HIGH-PRESSURE COMPRESSOR

Parameter	Method			Maximum difference, percent
	E^3 drawing	WATE	Finite difference	
Weight, lb	37.69	45	29.8	33.8
Material	Ti-6Al-4V	Ti-6Al-4V	Ti-6Al-4V	(b)
Life, cycles	(a)	(a)	150 000	
Average safety margin	(a)		0.06	
Safety margin	(a)		0.11	
r_1, in.	4.30		3.44	
$t_2 = t_1$, in.	1.00		0.91	
r_2, in.	4.90		3.74	
r_3, in.	6.10		3.93	
$t_4 = t_3$, in.	0.20		0.08	
r_4, in.	8.00		9.04	

[a]Not provided.
[b]Not applicable.

Advanced Subsonic Engine's high-pressure compressor consumed approximately 10 min on an IBM–RISC6000 computer. Depending on the geometry and loads of the rotating disks, the number of users on the computer, and the magnitudes (memory usage and CPU time usage) of the computer batch jobs, the elapsed time for the computer program in this study can vary from 5 min to 1 hr.

Concluding Remarks

A methodology was developed for structurally designing the rotating disks of an aircraft engine. The structural design methodology, along with a previously derived methodology for predicting low-cycle fatigue life was implemented in a

computer program. An interface computer program was also developed for this study that gathers all the required data from a flowpath analysis program currently used by NASA Lewis. The computer program developed for this study requires no interaction with the user and can be used as a postprocessor of the flowpath analysis program. The computer program was verified and validated by employing the finite element analysis method; the differences between the stresses and displacements obtained from the results of this study and the finite element analysis were all below 3%.

Future work should consist of

(1) Developing the methodology for a thermal transient analysis of rotating disks and implementing this methodology through a computer program. This work should be interfaced with the computer program developed for this study so that the thermal loads are automatically input.

(2) Developing a temperature-dependent material property subroutine and adding more superalloy materials to the material subroutine.

Lewis Research Center
National Aeronautics and Space Administration
Cleveland, Ohio, May 19, 1995.

References

1. Manson, S.S.: Determination of Elastic Stresses in Gas-Turbine Disks. NACA TN 871, 1947.
2. Millenson, M.B.; and Manson, S.S.: Determination of Stresses in Gas-Turbine Disks Subjected to Plastic Flow and Creep. NACA TN 906, 1948.
3. Mendelson, A.; and Manson, S.S.: Practical Solution of Plastic Deformation Problems in Elastic-Plastic Range. NACA TN 4088, 1957.
4. Manson, S.S.: Fatigue: A Complex Subject—Some Simple Approximations. J. Exp. Mech., vol. 5, no. 7, July 1965.
5. Seely, F.B.; and Boresi, A.P.: Advanced Mechanics of Material. Third ed.,Wiley, 1978.
6. McKnight, R.L: Personal telephone conversation. General Electric Aircraft Engine Group, July 1994.
7. Na, T.Y.: Computational Methods in Engineering Boundary Value Problems. Academic Press, New York, 1979.
8. Onat, E.; and Klees, G.W.: A Method to Estimate Weight and Dimensions of Large and Small Gas Turbine Engines. NASA CR–159481, 1979.
9. Coffin, L.F.: Study of Effects of Cyclic Thermal Stresses on Ductile Metal. Trans. ASME, vol. 76, no. 6, discussion, Aug. 1954, pp. 931–949.
10. McKnight, R.L.: DISKP—AEG 600 Time-Sharing System for Cyclic Plastic Analysis of Rotating Discs. General Electric Technical Information Series No. R70AEG284, May 1970.
11. Military Standardization Handbook. Metallic Materials and Elements for Aerospace Vehicle Structures. MIL–HDBK–5D, vol. 1, June 1983.
12. Manson, S.S.: Aerospace Structural Metals Handbook. AFML–TR–68–115, Code 4103, Nonferrous Alloys, March 1974.
13. Engineering Design Guide, Rotating Machinery. Engineering Directorate, NASA Lewis Research Center, vol. 2, 1994.
14. Cruse, T.: Personal telephone conversation. University of Vanderbilt, June 1994.
15. Miura, H.; and Schmit, L.A., Jr.: NEWSUMT: A FORTRAN Program for Inequality Constrained Function Minimization. (California Univ.; NASA Contract NGR–05–007–337.) NASA CR–159070, June 1979.
16. Timoshenko, S.; and Goodier, J.N.: Theory of Elasticity. Third ed., McGraw-Hill Publishing Co., 1987.
17. Joseph, J.A.: MSC/NASTRAN User's Manual. The MacNeal-Schwendler Corp., 1984.
18. Buttler, L.:Personal telephone conversation. General Electric Aircraft Engine Group, Jan. 1995.

REPORT DOCUMENTATION PAGE

Form Approved
OMB No. 0704-0188

1. AGENCY USE ONLY (*Leave blank*)	2. REPORT DATE	3. REPORT TYPE AND DATES COVERED
	November 1995	Technical Memorandum

4. TITLE AND SUBTITLE

Structural Optimization Methodology for Rotating Disks of Aircraft Engines

5. FUNDING NUMBERS

WU-505-69-50

6. AUTHOR(S)

Sasan C. Armand

7. PERFORMING ORGANIZATION NAME(S) AND ADDRESS(ES)

National Aeronautics and Space Administration
Lewis Research Center
Cleveland, Ohio 44135-3191

8. PERFORMING ORGANIZATION REPORT NUMBER

E-9598

9. SPONSORING/MONITORING AGENCY NAME(S) AND ADDRESS(ES)

National Aeronautics and Space Administration
Washington, D.C. 20546-0001

10. SPONSORING/MONITORING AGENCY REPORT NUMBER

NASA TM-4693

11. SUPPLEMENTARY NOTES

Responsible person, Sasan C. Armand, organization code 2410, (216) 977-7040.

12a. DISTRIBUTION/AVAILABILITY STATEMENT

Unclassified - Unlimited
Subject Category 37

This publication is available from the NASA Center for Aerospace Information, (301) 621-0390.

12b. DISTRIBUTION CODE

13. ABSTRACT ***(Maximum 200 words)***

In support of the preliminary evaluation of various engine technologies, a methodology has been developed for structurally designing the rotating disks of an aircraft engine. The structural design methodology, along with a previously derived methodology for predicting low-cycle fatigue life, was implemented in a computer program. An interface computer program was also developed that gathers the required data from a flowpath analysis program (WATE) being used at NASA Lewis. The computer program developed for this study requires minimum interaction with the user, thus allowing engineers with varying backgrounds in aeropropulsion to successfully execute it. The stress analysis portion of the methodology and the computer program were verified by employing the finite element analysis method. The 10th-stage, high-pressure-compressor disk of the Energy Efficient Engine Program (E^3) engine was used to verify the stress analysis; the differences between the stresses and displacements obtained from the computer program developed for this study and from the finite element analysis were all below 3% for the problem solved. The computer program developed for this study was employed to structurally optimize the rotating disks of the E^3 high-pressure compressor. The rotating disks designed by the computer program in this study were approximately 26% lighter than calculated from the E^3 drawings. The methodology is presented herein.

14. SUBJECT TERMS	15. NUMBER OF PAGES
Structural optimization methodology; Rotating disks	18
	16. PRICE CODE: A03

17. SECURITY CLASSIFICATION OF REPORT	18. SECURITY CLASSIFICATION OF THIS PAGE	19. SECURITY CLASSIFICATION OF ABSTRACT	20. LIMITATION OF ABSTRACT
Unclassified	Unclassified	Unclassified	

National Aeronautics and
Space Administration

Lewis Research Center
21000 Brookpark Rd.
Cleveland, OH 44135-3191